Loss of TRPM8 Exacerbate Herpes Simplex Keratitis Infection in Mice by Promoting the Infiltration of CD11b$^+$ Ly6G$^+$ Cells and Increasing the Viral Load in the Cornea

Jing Feng,[1] Lingling Yang,[1] Lili Ran,[1,2] Xia Qi,[1] Xiaolei Wang,[1] Yangyang Zhang,[1] Zongzheng Zou,[1] Ting Liu,[1] Xiaochuan Wang,[1] Yang Yu,[1] Xiaodong Sun,[1] and Qingjun Zhou[1]

[1]State Key Laboratory Cultivation Base, Shandong Provincial Key Laboratory of Ophthalmology, Eye Institute of Shandong First Medical University, Qingdao, China
[2]Qingdao University Medical College, Qingdao University, Qingdao, China

Correspondence: Qingjun Zhou, State Key Laboratory Cultivation Base, Shandong Provincial Key Laboratory of Ophthalmology, Eye Institute of Shandong First Medical University, Yanerdao Road, Qingdao 266071, China; qjzhou2000@126.com.

Received: April 14, 2023
Accepted: October 30, 2023
Published: December 20, 2023

Citation: Feng J, Yang L, Ran L, et al. Loss of TRPM8 exacerbate herpes simplex keratitis infection in mice by promoting the infiltration of CD11b$^+$ Ly6G$^+$ cells and increasing the viral load in the cornea. *Invest Ophthalmol Vis Sci.* 2023;64(15):24. https://doi.org/10.1167/iovs.64.15.24

Purpose. To reveal the role of transient receptor potential cation subfamily M member 8 (TRPM8) channels in herpes simplex keratitis (HSK).

Methods. HSK models were established using TRPM8 knockout (TRPM8$^{-/-}$) mice and their wild-type (WT) littermates. The infected corneas were graded and harvested to evaluate the mRNA levels of inflammatory factors through quantitative real-time polymerase chain reaction (RT-PCR), as well as the infiltration of inflammatory cells through immunofluorescence staining and flow cytometry. Viral titers were determined by plaque assay and absolute quantitative method. RNA-sequencing was conducted to elucidate the transcriptome of corneal epithelium in response to TRPM8 knockout after infection. The anti-inflammatory effect of TRPM8 agonist menthol was documented via subconjunctival administration.

Results. Compared to their wild-type counterparts, TRPM8-deficient mice exhibited exacerbated infection symptoms and thicker corneas in HSK models. Infection in TRPM8-deficient mice resulted in significant lymphocyte infiltration, primarily consisting of Ly6G$^+$ CD11b$^+$ cells. Additionally, TRPM8-deficient mice displayed increased levels of corneal viral titers after infection, along with decreased expression of interferon-stimulated genes (ISGs). Subconjunctival administration of menthol effectively alleviated infection-induced symptoms and Ly6G$^+$ CD11b$^+$ cell infiltration in herpes simplex virus type 1 (HSV-1)–treated mice.

Conclusions. TRPM8 promoted host resistance to HSV-1 infection by suppressing the accumulation of Ly6G$^+$ CD11b$^+$ cells and virus replication. These findings suggest that targeting TRPM8 could be valuable for therapeutic interventions against HSV-1 infections.

Keywords: TRPM8, HSK, Ly6G$^+$ CD11b$^+$ cells, ISG

Herpes simplex keratitis (HSK) is a significant cause of vision loss worldwide, caused by herpes simplex virus type 1 (HSV-1).[1] HSK is characterized by a high incidence of blindness and recurrent episodes, resulting in visual impairment and imposing heavy psychological and economic burdens on both patients and society.[2]

The Corneal TRPM8 channel is implicated in cold sensation,[3,4] pain sensation,[5] corneal epithelial wound healing,[6] and the mediation of tear secretion.[7,8] Recent studies have indicated that TRPM8 can modulate the immune response,[9] including in the skin,[10] lung,[11] and intestine,[12–14] as well as affect Coxsackievirus B replication.[15] Activation of TRPM8 induces an increase in interleukin-10 release, a reduction in tumor necrosis factor release by macrophages[16,17] and is beneficial for T-cell activation[18] and differentiation into effector cells.[19] Moreover, TRPM8 has been reported to inhibit the release of neuropeptide from sensory neurons and exert effects on CD11c$^+$ dendritic cells to alleviate experimental colitis.[13] Additionally, natural agonists of TRPM8 have been utilized for the treatment of various inflammatory conditions and viral infections. Thymol alleviates the inflammatory response in imiquimod-treated mice.[10] Eucalyptol attenuates edema and mechanical allodynia in the footpad inflammation.[20] Menthacarin attenuates experimental colitis.[21] Thymol, menthol, and 1,8-cineole can reduce virus infectivity on cells.[15,22–24] Despite accumulating evidence suggesting that TRPM8 plays an important part in regulation of the inflammatory response and virus infection, its involvement in HSK remains unclear.

In this investigation, our aim was to investigate the potential role of TRPM8 in the pathogenesis of HSK. To achieve this objective, we used TRPM8-deficient mice and their wild-type littermates to establish HSK models and subsequently evaluated the impact of TRPM8 deficiency on

infection severity, immune cell infiltration, and viral replication. Additionally, we performed RNA sequencing to unravel changes in the transcriptome of corneal epithelial cells in response to TRPM8 knockout after infection. Our results may offer novel insights into the underlying mechanisms of HSK and propose TRPM8 as a promising therapeutic target for HSK.

Material and Methods

Animal

TRPM8$^{-/-}$ mice were obtained from Jackson Laboratory (catalog number: 008198; Sacramento, CA, USA). Adult male C57BL/6 mice were purchased from the Beijing HFK Bioscience (Beijing, China) and housed in the Animal Center of Shandong Eye Institute. The mice used in this study weighed between 18 and 22 g and had normal eye development. All animal procedures were conducted in accordance with the ARVO Statement and Committee guidelines of the Shandong Eye Institute for the Use of Animals in Ophthalmic and Vision Research.

Culture and Amplification of HSV-1 and Establishment of HSK Model

HSV-1 was replicated on Vero cells, and its titer was measured using a plaque assay. In brief, cells were inoculated in 24-well plates at a concentration of 1×10^5. The collected virus solution was diluted to infect the cells accordingly. A cover layer was created using Dulbecco's modified Eagle medium-F12 solution containing 0.6% agar and 2% fetal bovine serum. Finally, the virus titer was determined by counting the number of plaques formed by virus (pfu/mL). The HSK model was established by scratching the corneal surface of male mice with a 30-G needle in a crosshatch pattern consisting of 20 vertical and 20 horizontal scratches, followed by administration of the McKrae strain of HSV-1 with a titer of 1×10^6 pfu.[25,26]

Corneal photographs were taken using a slit-lamp microscope (SL-D701; Topcon, Tokyo, Japan). The assessment of corneal keratitis severity includes opacity and corneal neovascularization (CNV) as previously described.[27,28] Briefly, corneal opacity was graded on a standard scale ranging from 0 to 5: 0 = transparent; 1 = mildly cloudy (a slight cloudy area could be vaguely identified, and the iris and pupil can be clearly seen); 2 = moderate opacity (the cloudy area could be identified easily, and the details of the iris and pupil could be partly observed); 3 = severe opacity (the details of the iris and pupil were obstructed by the opacity area, but the brown iris could still be distinguished from the black pupil); 4= most severe opacity (observation of the iris and pupil was blocked by the opacity area); 5 = corneal rupture. To quantify opacity, anterior segment optical coherence tomography (OCT) images were analyzed by measuring the average pixel intensity.[29,30] Additionally, the cornea is divided into four quadrants, and CNV for each eye is calculated as the sum of scores for all four quadrants. The length of CNV in each quadrant is graded from 0 to 4, with increments of approximately one quarter of the corneal radius. After corneal flatmount staining, the degree of neovascularization (CD31$^+$ area as a percentage of the total corneal area) was then quantified.

Corneal Thickness Measurements

The central corneal thickness was measured using OCT (RTVue XR 100, version 2018.1.0.43; Optovue, Inc., Fremont, CA, USA) with a long adaptor lens for the corneal anterior module (maximum scan depth of 2.4 mm and scan width of 8.0 mm).[6] The cross-line mode was used to capture sagittal images of the central cornea, and the ruler tool provided with the instrument was used to calculate corneal thickness. The entire acquisition and measurement were performed in a blinded manner by two trained ophthalmic examiners.

Flow Cytometry

After euthanasia, the eyeballs of each mouse were harvested, and a single-cell suspension of the cornea was prepared. The epithelium was separated from the stromal endothelium using dispase II (15 mg/mL) at 37°C for two to three hours. Subsequently, trypsin and collagenase (10103586001; Roche, Basel, Switzerland) were used to digest the corneal epithelium and stroma, respectively. Then the cells were collected and washed in a single-cell state. The primary antibody and the corresponding control isotype IgG were added for a light-protection reaction at 4°C for 30 minutes. The following anti-mouse antibodies (all from BioLegend, San Diego, CA, USA) were used: Ly6G-fluorescein isothiocyanate (108406), anti-mouse/human-CD11b-APC (101212) and anti-mouse-CD45-Percp/Cyanine 5.5 (103131). FSC-A and SSC-A gating strategies were used to exclude cell debris. To discriminate doublets, FSC-A was aligned against FSC-H, and the appropriate gating was applied. Before analysis, cells were treated with 7-AAD, and dead cells labeled with 7-AAD$^+$ were excluded from further analysis. Cells were washed and filtered and then counted by a FACSCalibur flow cytometer (CytoFLEX; Beckman Coulter, Fullerton, CA, USA). Data analysis was performed using CytExpert and Flowjo10.0.

Staining

Hematoxylin and eosin (H&E) staining was carried out according to a conventional protocol. Briefly, after dewaxing and rehydration, tissue paraffin sections were stained with hematoxylin solution (ZSGB-BIO, Beijing, China) for five minutes. Subsequently, they were immersed in 1% acidic ethanol (1% HCl in 75% ethanol) for five minutes and rinsed with distilled water. The sections were then stained with eosin solution (ZSGB-BIO, Beijing, China) for three minutes, dehydrated using a graded series of alcohol solutions, and clarified in xylene. For immunofluorescence staining, fresh corneas were collected and embedded in optimal cutting temperature compound (14020108926; Leica, Wetzlar, Germany). Tissue sections of thickness 7 µm were obtained using a freezing microtome (CM 1950; Leica), fixed with 4% (*w/v*) paraformaldehyde for 10 minutes, permeabilized with 0.3% (*v/v*) Triton x-100, and blocked in 10% goat serum for one hour. After thorough washing steps, the samples were incubated overnight at 4°C in a humidified chamber with primary antibodies. After this step, the corresponding secondary antibody (1:1000 dilution) was applied to the samples for two hours at room temperature. Nuclei were counterstained using DAPI dye. The primary antibodies used included TRPM8 (1:1000 dilution; ab10938; Abcam, Cambridge, MA, USA), F4/80 (1:200 dilution; 123108; BioLe-

Investigative Ophthalmology & Visual Science

Table. Primers Used for qPCR

Gene	Forward Primer	Revers Primer
Rpl5	CCGCAGGCTTCTGAATAGGTCCGCAGGCTTCTGAATAGGT	CCAGTTGTAGTTCGGGCAAGA
Ccl2	CAGCAAGATGATCCCAATGAGTAG	TTTTTAATGTATGTCTGGACCCATTC
Ccl3	TGCCTGCTGCTTCTCCTACA	TGGACCCAGGTCTCTTTGGA
Cxcl2	GGCTGTTGTGGCCAGTGAA	ACTTTTTGACCGCCCTTGAGA
Cxcl1	TGTCAGTGCCTGCAGACCAT	CAAGGGAGCTTCAGGGTCAA
Il-1β	CTTTCCCGTGGACCTTCCA	CTCGGAGCCTGTAGTGCAGTT
Il-6	GAGGATACCACTCCCAACAGACC	AAGTGCATCATCGTTGTTCATACA
TK	AAGGTCGGCGGGATGAG	CGGCCGCGCGATAC
VP16	GCGGGGCCGGGATTTACC	CTCGAAGTCGGCCATATCCA
ICP27	GCATCCTTCGTGTTTGTCATT	GCATCTTCTCTCCGACCCCG
Oas1a	GGAGCTCCAGCGGAACTTC	CAGGCAAAGACAGTGAGCAACT
Ccl5	GACACCACTCCCTGCTGCTT	CTTCTCTGGGTTGGCACACA
Irf7	CACCCCCATCTTCGACTTCA	TCACCAGGATCAGGGTCTTCTC
Mx1	CAGAAGATGACAGAACGAGGATGT	CCCAAGCAAGAAACTCATTTCG
H2-M3	GCACAAAGTGCCAGAGCAAA	GCCATCATACGCAGCCTGAT
Rsad2	TCTGCTCAAACAGGCTGGTTT	AGGCTGCCATTGCTCACTATG

gend, San Diego, CA, USA), HSV-1 (1:1000 dilution; ab9533; Abcam) and LY6G (1:200 dilution; 108406; BioLegend).

Corneal flat-mount staining was performed to quantify the extent of blood vessel coverage in the cornea. The eyeballs were extracted and fixed in 4% paraformaldehyde at 4°C for 15 minutes. Subsequently, the cornea was separated from the eyeball and fixed at 4°C for two hours. After being blocked with a PBS solution containing 0.3% Triton and 5% donkey serum at room temperature for one hour, the corneas were incubated overnight at 4°C in a first antibody solution (1:200; AF3628-SP; R&D Systems, Minneapolis, MN, USA). After thorough washing, a secondary antibody (1:500) was applied and incubated at room temperature for an additional hour. Confocal laser scanning microscopy (Zeiss, Oberkochen, Germany) was used to analyze images, which were subsequently processed using Fiji ImageJ software (https://imagej.net/software/fiji/).

Quantitative Real-Time Polymerase Chain Reaction

The total RNA from cornea samples was extracted using TransZol Up Plus RNA Kit (ER501-01; Transgen Biotech, Beijing, China) according to manufacturer instructions. Complementary DNA was synthesized using the All-in-One First-Strand cDNA Synthesis SuperMix for qPCR (AE341-03; Transgen Biotech). RT-PCR was carried out using ChamQ SYBR qPCR Master Mix (Q341-02; Vazyme Biotech, Nanjing, China) and the 7500 Real Time PCR System (Applied Biosystems, Foster City, CA, USA). Pre-denaturation at 95°C for three minutes was followed by 40 two-step cycles consisting of denaturation at 95°C for five seconds and annealing/extension at 60°C for 30 seconds. Data analysis was conducted using sequence detection system software (Applied Biosystems), with glyceraldehyde-3-phosphate dehydrogenase serving as an internal control for mouse corneas (Table).

RNA Sequencing and Gene Ontology Analysis

The corneal epithelia were collected three days post-infection (dpi), and RNA extraction was performed using TransZol Up Plus RNA Kit (ER501-01; Transgen Biotech, Beijing, China) following the manufacturer instructions. Each sample originated from the corneal epithelium of three mice. RNA sequencing and transcriptomic data processing were conducted by Capitalbio Technology Inc. (Beijing, China). Briefly, the bcl2fastq software is used to perform base calling on raw image files from Illumina high-throughput sequencing, converting the resulting sequenced reads into raw sequencing sequences for subsequent analysis. The sequencing data were cleaned and filtered using fastp software and quality controlled by FastQC. Clean reads were then aligned to the reference genome sequence using HISAT2/tophat2. Genes and transcript reconstruction were performed using StringTie. Readcount calculation for expression levels was performed using featureCounts or Stringtie. A differential expression analysis was performed using the DESeq method. Genes with an adjusted p-value < 0.05 and an absolute value of $|\log2FoldChange| > 1$ were assigned as significant differentially expressed genes (DEGs). A Gene ontology (GO) enrichment analysis and the heat map were generated using the OECloud tools available at https://cloud.oebiotech.com.

Drug

The stock solution of 100 mM TRPM8 agonist menthol (HY-75161; MedChemExpress, Monmouth Junction, NJ, USA) was prepared in a mixture containing 10% DMSO, 40% PEG300, 5% Tween-80, and 45% saline solution. The stock solution was then further diluted with saline solution to a concentration of 100 µM. The same final solution without menthol was used as a control that contains 0.1% DMSO, 0.4% PEG300, and 0.05% Tween-80 in saline solution. Both the menthol and control solutions were administered subconjunctivally at a volume of 5 µL per eye per day starting from −1 dpi.

Statistical Analyses

Prism 8 (GraphPad, San Diego, CA, USA) was used for data analysis. Data were obtained from at least triplicate experiments and presented as mean ± standard error in the figures. Normal distribution was observed in the data, and hence unpaired *t*-test was used to compare two groups. One-way ANOVA was used to assess differences among multiple groups. Statistical significance was considered at $P < 0.05$ (ns, no significance; $^{*}P < 0.05$; $^{**}P < 0.01$; and $^{***}P < 0.001$).

Investigative Ophthalmology & Visual Science

All experiments were validated with a minimum of three replicates.

Results

The Loss of TRPM8 Exacerbates Keratitis Caused by Herpes Simplex Virus-1

To reveal the roles of TRPM8 in HSV-1 infection, a murine model of HSK was established utilizing TRPM8$^{-/-}$ mice and WT mice. The TRPM8$^{-/-}$ mice exhibited exacerbated HSK symptoms post-infection (Fig. 1A), characterized by increased corneal opacity and neovascularization. In TRPM8$^{-/-}$ mice (2.615 ± 0.29 at 3 dpi and 3.538 ± 0.351 at 6 dpi), corneal opacity was significantly increased compared to the control group (1.231 ± 0.281 at 3 dpi and 2.154 ± 0.337 at 6 dpi) at 3 dpi and 6 dpi (Fig. 1B). Quantitative analysis of pixel intensity on anterior segment OCT images yielded consistent findings (111.5 ± 4.834 in WT mice and 130.3 ± 3.550 in TRPM8$^{-/-}$ mice) at 3 dpi (Fig. 1C). In the context of angiogenesis, a notable disparity was observed between the TRPM8$^{-/-}$ group and WT control mice, as the former exhibited earlier onset of angiogenesis compared to the latter (Fig. 1D). At 6 dpi and 10 dpi, the score of corneal neovascularization in the TRPM8$^{-/-}$ group (5 ± 0.817 at 6 dpi and 11.15 ± 1.568 at 10 dpi) was significantly higher than that of the WT control group (1.692 ± 0.511 at 6 dpi and 6.538 ± 1.555 at 10 dpi). The percentage of neovascularization area in relation to total corneal area was greater in the TRPM8$^{-/-}$ group (45.74% ± 4.229%) than in the WT group (23.73% ± 2.621%) at 6 dpi (Fig. 1E and Supplementary Fig. S1).

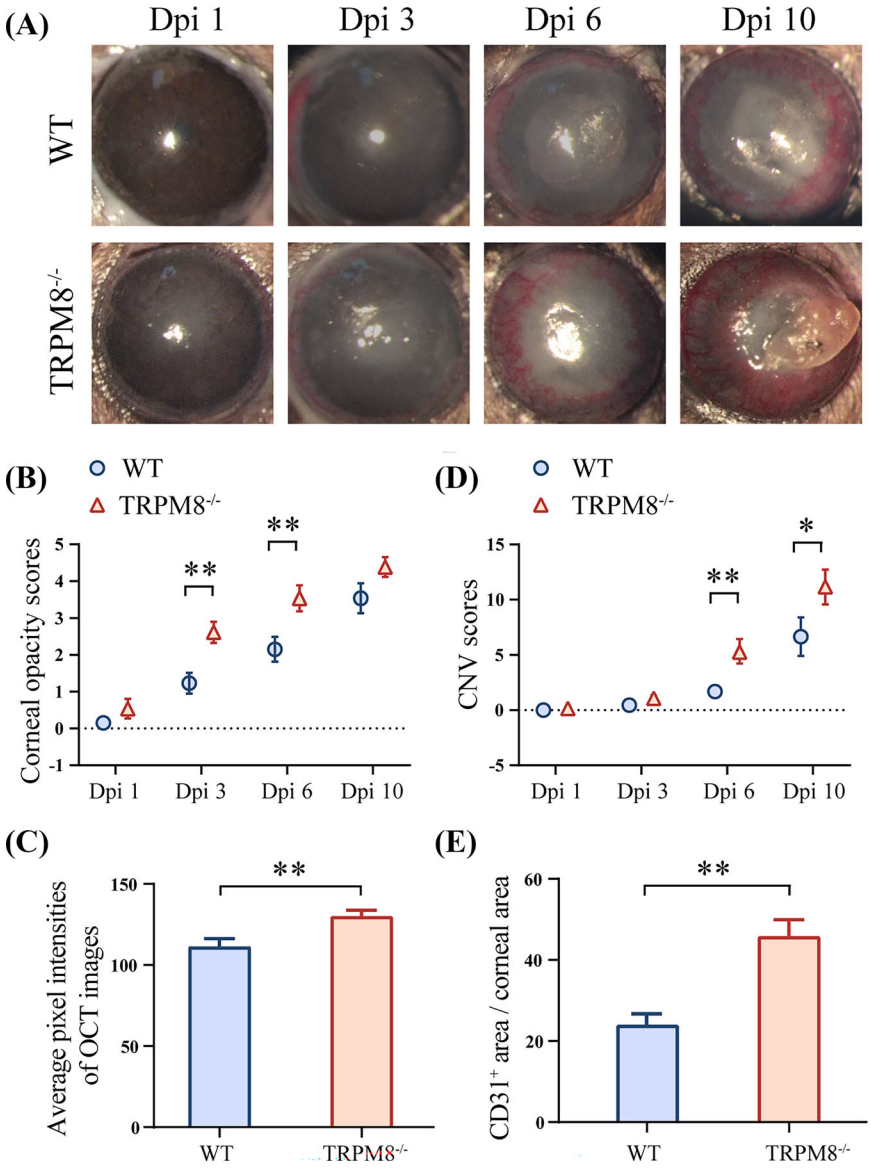

Figure 1. The susceptibility of TRPM8$^{-/-}$ mice to HSV-1 infection increased. (**A**) Representative images of progression of corneal lesions in WT mice (top line) and TRPM8$^{-/-}$ mice (bottom line). (**B**) Statistical analysis of corneal opacity scores (n = 13 per group). $^{**}P < 0.01$. (**C**) The quantitation of corneal opacity obtained in optical coherence tomography (OCT) images with respect to pixel intensity (n = 14, WT; n = 9, TRPM8$^{-/-}$, 3 dpi). $^{**}P < 0.01$. (**D**) Statistical analysis of CNV scores (n = 13 per group). $^{**}P < 0.01$; $^{*}P < 0.05$. (**E**) The quantitation of CD31-stained area in corneal flat mounts staining (n = 4 per group, 6 dpi). $^{**}P < 0.01$.

Investigative Ophthalmology & Visual Science

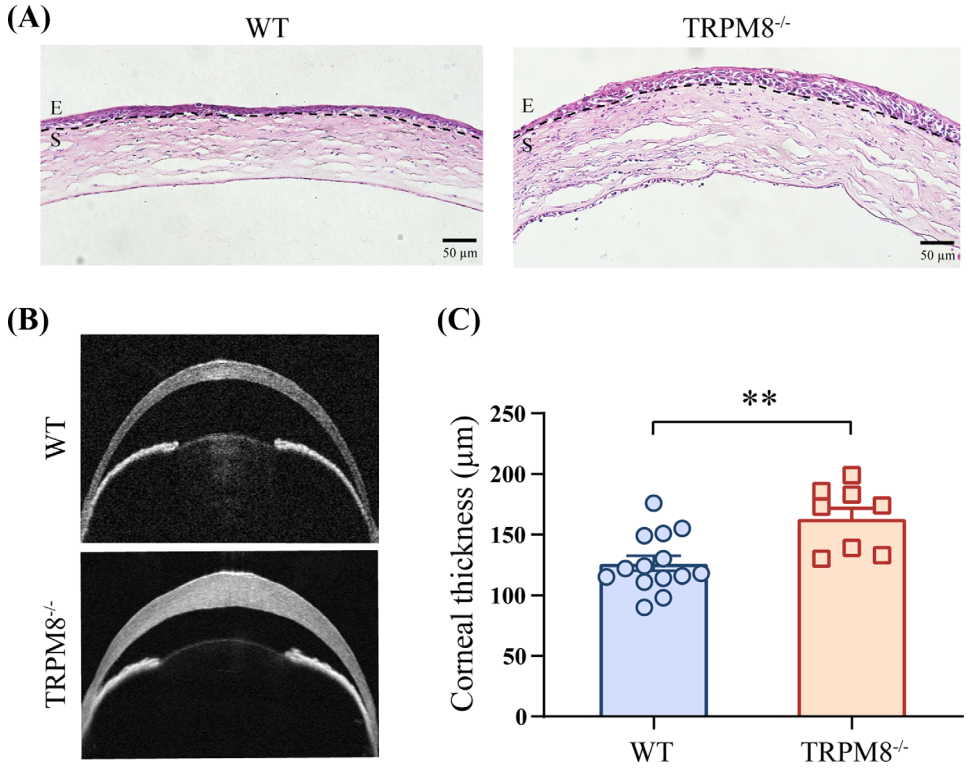

Figure 2. The corneas of TRPM8$^{-/-}$ mice were thicker three days after HSV-1 infection compared with those in WT mice. (**A**) H&E staining of corneas. E, epithelium; S, stroma. Results are from at least one of three independent experiments. (**B**) Representative images of corneal anterior segment OCT in WT mice (top line) and TRPM8$^{-/-}$ mice three days after HSV-1 infection. (**C**) Comparison of corneal thickness (n = 14, WT, 3 dpi; n = 9, TRPM8$^{-/-}$, 3 dpi). Data are the mean ± SEM. $^{**}P < 0.01$.

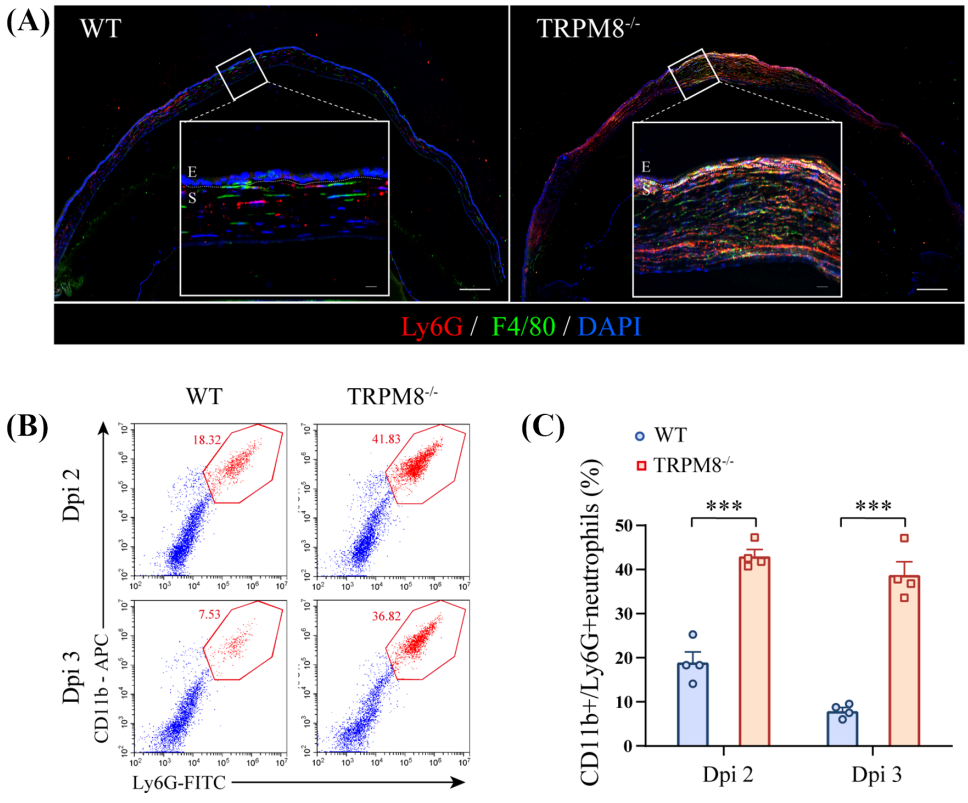

Figure 3. Recruitment and high persistence of CD11b^{+} Ly6G^{+} cells in TRPM8$^{-/-}$ mice in HSK. (**A**) Immunofluorescence for F4/80^{+} macrophages (*green*), Ly6G^{+} cells (*red*), and DAPI (*blue*) (*Scale bar*: 150 μm; E, epithelium; S, stroma) at dpi 3. *White outlined insets* show high-magnification images of the indicated regions (*Scale bar*: 25 μm; E, epithelium; S, stroma). Images were obtained from at least one of three independent experiments. (**B**) Representative dot plots of the percentage of CD11b^{+} Ly6G^{+} cells in the cornea analyzed 2 dpi and 3 dpi by flow cytometry in WT mice and TRPM8$^{-/-}$ mice. (**C**) Percentage of CD11b^{+} Ly6G^{+} cells in the cornea in WT mice and TRPM8$^{-/-}$ mice (n = 4 mice per group). Data are the mean ± SEM. $^{***}P < 0.001$.

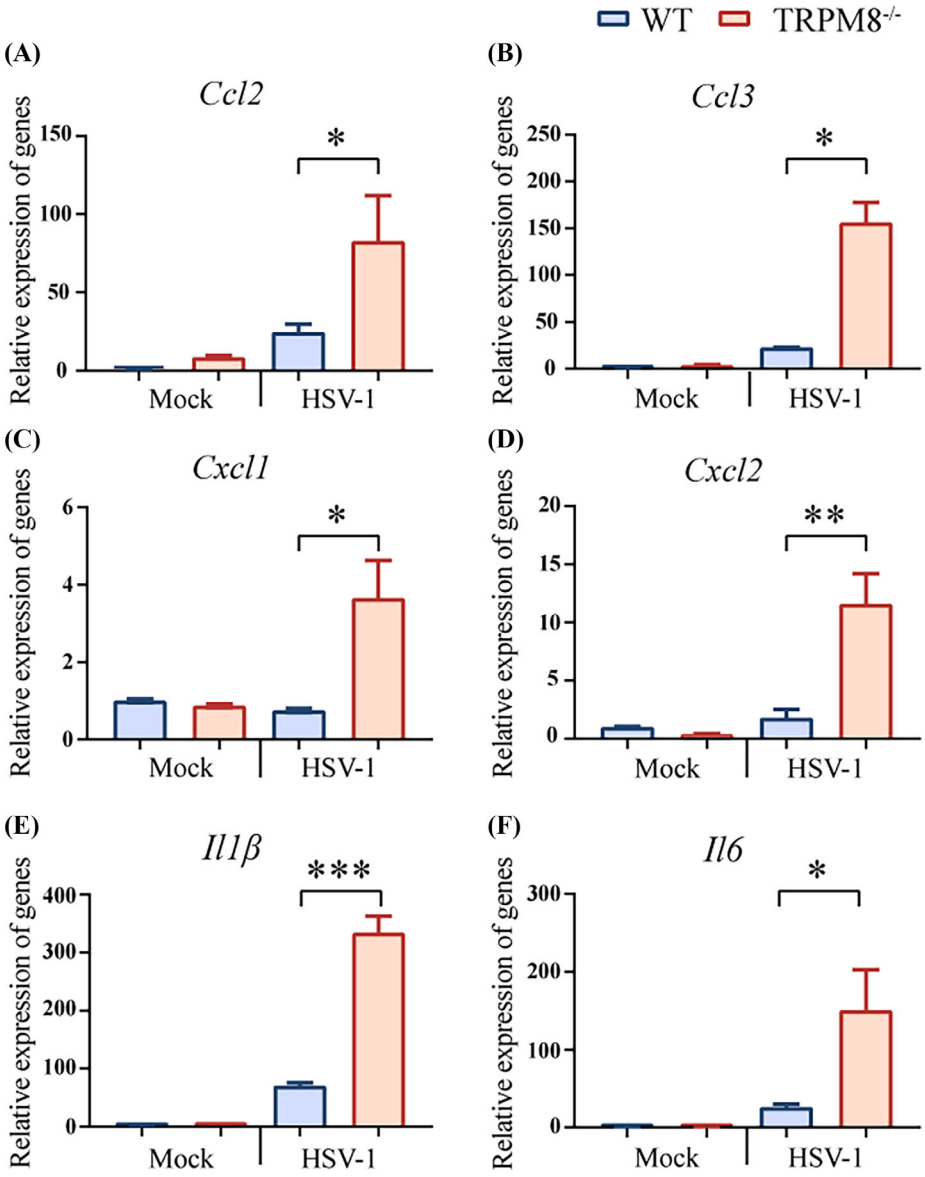

Figure 4. TRPM8 knockdown resulted in upregulated chemokine expression in mice after infection. (**A–D**) The gene expression of chemokine Ccl2, Ccl3, Cxcl1, Cxcl2 in cornea homogenates of WT mice and TRPM8$^{-/-}$ mice three days after HSV-1 infection or in mock-infected mice. Results are from one of three independent experiments (n = 3 mice per group). *$P < 0.05$, **$P < 0.01$. (**E**, **F**) The gene expression of cytokine IL-1β and IL-6 in cornea homogenates of WT mice and TRPM8$^{-/-}$ mice three days after HSV-1 infection or in mock-infected mice. Data from one of three independent experiments are the mean ± SEM (n = 3 mice per group). *$P < 0.05$. ***$P < 0.001$.

The Loss of TRPM8 Promotes Corneal Thickening After HSV-1 Infection

The infection of HSV-1 resulted in an enhanced recruitment of leukocytes to the corneas.[31,32] H&E staining showed more focal inflammatory cells infiltrating in TRPM8$^{-/-}$ mice 3 dpi with HSV-1 compared with that in WT mice (Fig. 2A). After HSV-1 infection, the central corneal thickness was significantly increased in the TRPM8$^{-/-}$ group (163.3 ± 8.425 µm) compared to the WT group (126.4 ± 6.317 µm) 3 days after infection (Figs. 2B, 2C).

TRPM8 Deletion Promotes the Infiltration of CD11b^{+} Ly6G^{+} Cells After HSV-1 Infection

Because the increased leukocyte infiltration in TRPM8$^{-/-}$ mice, flow cytometry was undertaken to further identify the composition of inflammatory-cell types. Corneal cells were isolated from infected TRPM8$^{-/-}$ mice and WT mice for analysis. Infected with HSV-1, TRPM8$^{-/-}$ mice had an increased percentage of infiltrating CD45^{+} CD11b^{+} Ly6G^{+} cells rather than CD45^{+} CD11b^{+} F4/80^{+} macrophages, CD45^{+} CD3^{+} T cells and CD45^{+} CD11c^{+} dendritic cells in CD45^{+} cells (Supplementary Fig. S2A). These observations were corroborated by immunofluorescence staining (Fig. 3A).

To identify the dynamics of CD11b^{+} Ly6G^{+} cells infiltration, corneas were harvested at various time points after infection and analyzed using flow cytometry. The dynamics of CD11b^{+} Ly6G^{+} cells infiltration during HSV-1 infection were assessed in WT mice. CD11b^{+} Ly6G^{+} cells migration to the cornea of infected WT mice began on 1 dpi, peaked at 2 dpi, and subsided slowly thereafter until 7 dpi (Supplementary Fig. S2B). Accordingly, we assessed the kinetics of CD11b^{+} Ly6G^{+} cells infiltration in both WT mice and

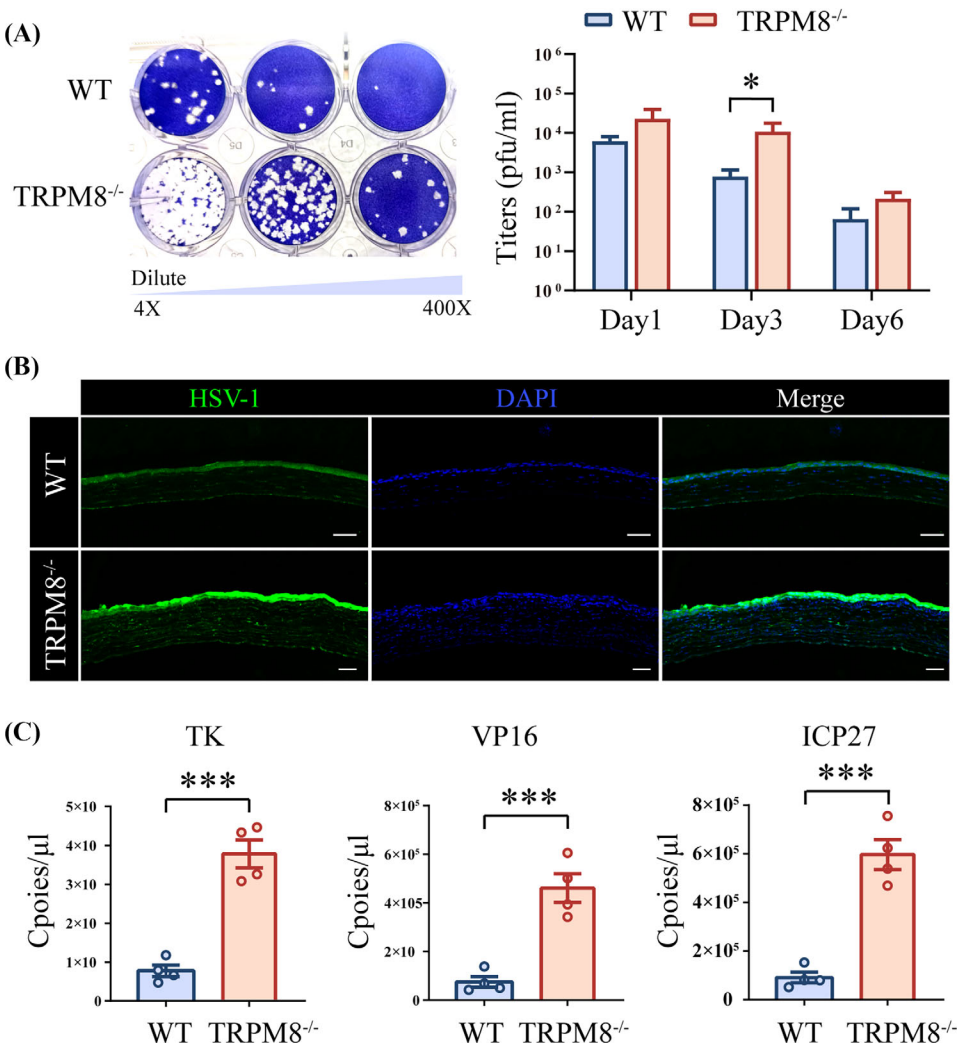

Figure 5. TRPM8$^{-/-}$ mice had an increased viral burden. (**A**) Representative result (*left panel*; 3 dpi) and statistical analysis (*right panel*; 1, 3, 6 dpi) of a plaque assay. The viral samples originated from WT mice (*top line*) and TRPM8$^{-/-}$ mice (*bottom line*) and were diluted ×4, ×40, and ×400. Results are from one of three independent experiments (n = 4 mice per group). *$P < 0.05$. (**B**) Representative pictures of corneal HSV-1 fluorescein staining. (**C**) Copies of TK, VP16, and ICP0 in cornea samples were measured by qPCR. *Rpl5* was used as the reference gene. Results are from one of three independent experiments (n = 4 mice per group). ***$P < 0.001$.

TRPM8$^{-/-}$ mice infected with HSV-1 at two days and three days (Fig. 3B). Gating strategy is described in Supplementary Figure S3. Compared to WT mice (19.01% ± 2.313%), TRPM8$^{-/-}$ mice (43.11% ± 1.434%) exhibited a significant increase in infiltrating CD11b^{+} Ly6G^{+} cells infiltrate starting from 2 dpi. Different from the control group (7.965% ± 0.7676%), there was no regression observed for CD11b^{+} Ly6G^{+} cell numbers at 3 dpi in TRPM8$^{-/-}$ mice (38.85% ± 2.908%) (Fig. 3C).

TRPM8 Deletion Promotes the Upregulation of Proinflammatory Cytokines and Chemokines After HSV-1 Infection

The infiltration of CD11b^{+} Ly6G^{+} cells into the cornea is regulated by chemoattractants, and HSV-1 infection leads to an increase in inflammatory factors.[2,33,34] Increased gene expression of chemokine in the cornea of TRPM8$^{-/-}$ mice infected with HSV-1 was observed, including chemokine (C-C motif) ligand 2 (Ccl2), chemokine (C-C motif) ligand 3 (Ccl3), chemokine (C-X-C motif) ligand 1 (Cxcl1), and chemokine (C-X-C motif) ligand 2 (Cxcl2) (Figs. 4A–D). To clarify the inflammatory factors affected by TRPM8, RT-PCR was undertaken to measure the gene expression of interleukin 1, beta (IL-1β), interleukin 6 (IL-6) in the cornea. Significant differences were observed in IL-1β and IL-6 expression after infection between wild-type mice and TRPM8$^{-/-}$ mice (Figs. 4E, 4F).

TRPM8$^{-/-}$ Mice Showed Increased Corneal Viral Burden

To evaluate the impact of TRPM8$^{-/-}$ on viral replication, we collected eye swabs from mice 1, 3, 6 days post-infection and quantified the titers in both TRPM8$^{-/-}$ and WT mice. Our results demonstrated that the virus titers in TRPM8$^{-/-}$ mice (14542 ± 5482 pfu/ml) were significantly higher than those in the WT mice (966 ± 355 pfu/ml)

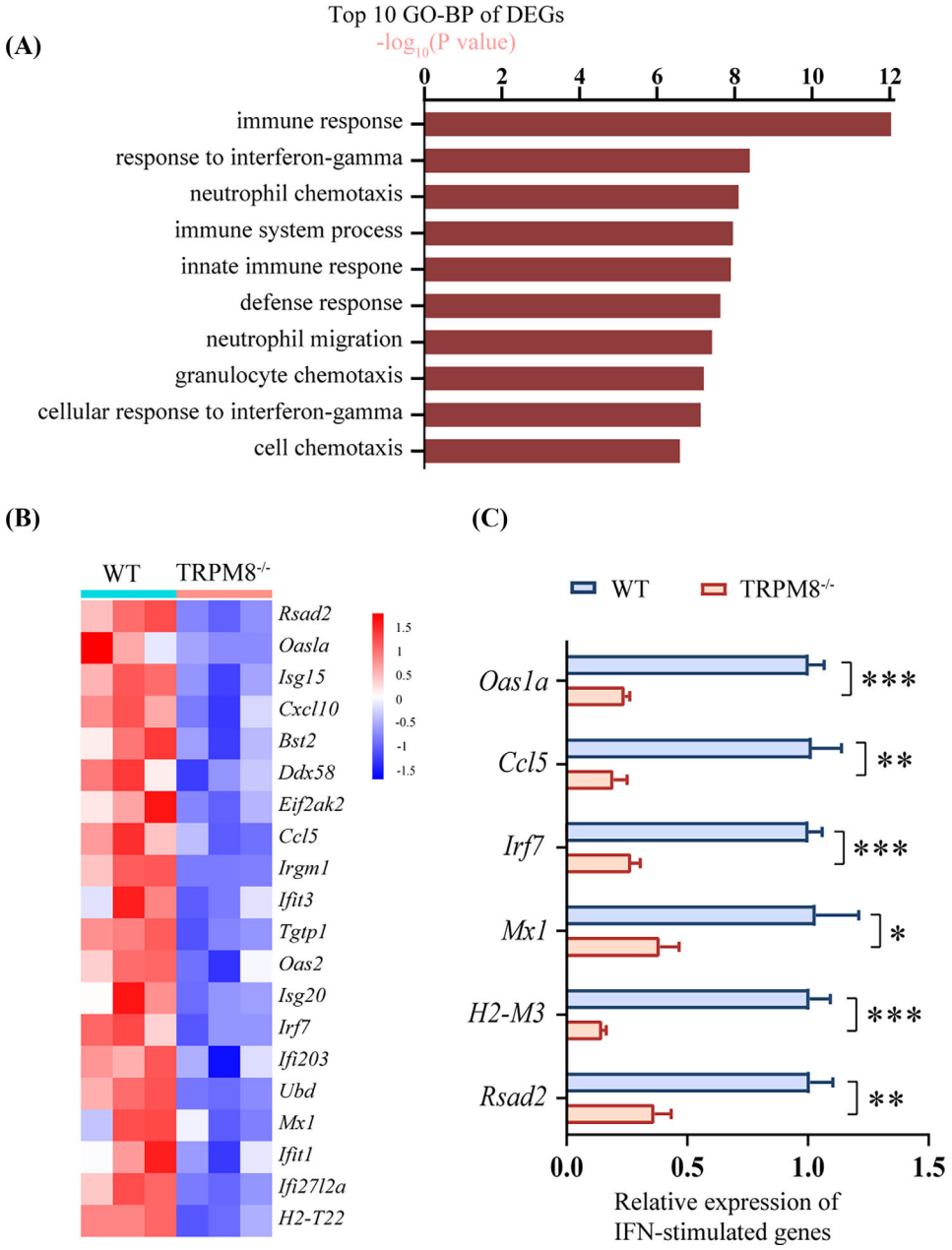

Figure 6. The expression of ISGs are significantly down-regulated in the corneas of TRPM8$^{-/-}$ mice compared with levels in WT mice. (**A**) Top 10 terms of the GO biological process enrichment analysis of DEGs. (**B**) Heatmap illustrating the significantly down-regulated ISGs in DEGs. (**C**) The qPCR validation of partial ISG expression was conducted. *P < 0.05; **P < 0.01; ***P < 0.001.

3 days post-infection (Fig. 5A). Furthermore, immune fluorescence staining revealed that the corneas of TRPM8$^{-/-}$ mice contained more virus, which was mainly concentrated in the corneal epithelium (Fig. 5B). To further validate our findings, we employed absolute quantitative PCR to assess viral titers in the corneas of these mice. Data showed that the transcript copies number of thymidine kinase (TK), tegument protein VP16 and immediate early protein ICP27 genes in the TRPM8$^{-/-}$ mice (378285 ± 35819 copies, TK; 460882 ± 58627 copies, VP16; 596835 ± 61617 copies, ICP27) were higher than those in the WT mice (77620 ± 14830 copies, TK; 74915 ± 21938 copies, VP16; 91278 ± 21754 copies, ICP27) 3 days post-infection (Fig. 5C).

TRPM8$^{-/-}$ Mice Exhibited a Downregulation of ISGS Expression

To investigate the underlying mechanism behind the increased corneal virus titers in TRPM8-deficient mice, we conducted RNA-seq analysis on cornea epithelial cells isolated from both WT and TRPM8$^{-/-}$ mice after HSV-1 infection. Compared with WT mice, there were 515 significant DEGs identified in TRPM8$^{-/-}$ mice, including 173 up-regulated and 342 downregulated genes (Supplementary Fig. S4). GO term analysis revealed that the top 10 enriched pathways were associated with immune responses, neutrophil chemotaxis, and responses to interferons, *etc.* (Fig. 6A). Additionally, we found that ISGs were

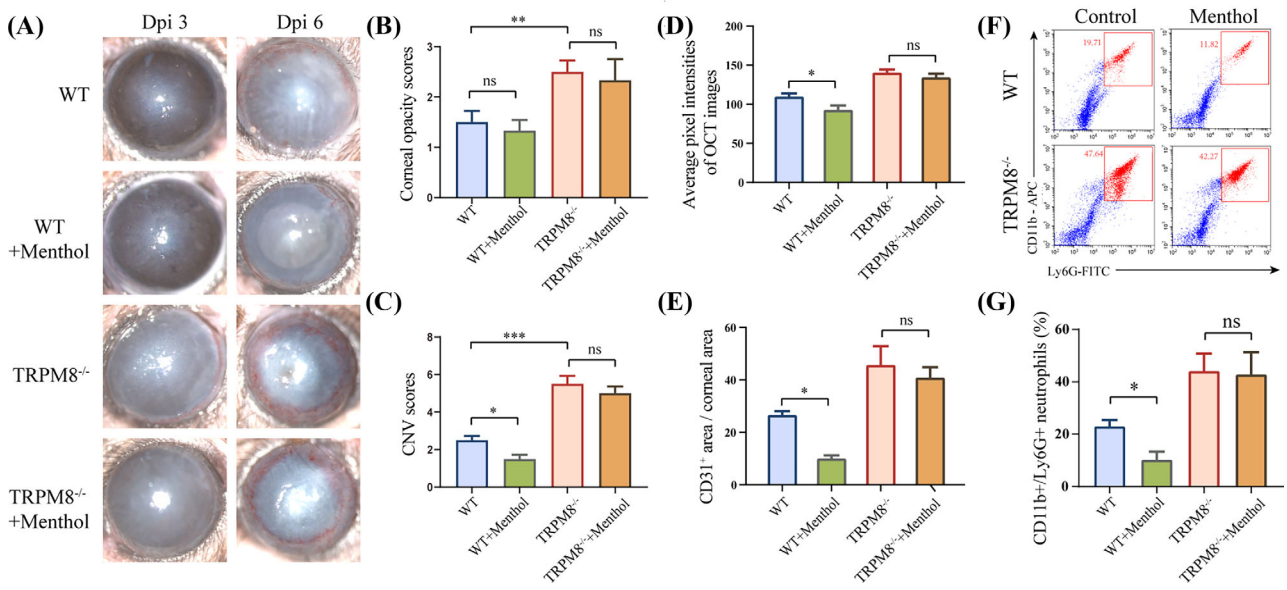

Figure 7. Therapeutic effect of TRPM8 agonist on the corneal inflammation wrought by HSV-1 infection. (**A**) Representative images of corneal lesions in WT mice and TRPM8$^{-/-}$ mice with or without subconjunctival administration of menthol (100 µM). (**B**) Statistical analysis of corneal opacity scores 3 dpi. (n = 8 per group). $^{**}P < 0.01$. (**C**) Statistical analysis of CNV scores 6 dpi (n = 8 per group). $^{***}P < 0.001$; $^{*}P < 0.05$. (**D**) The quantitation of corneal opacity obtained in OCT images with respect to pixel intensity 3 dpi (n = 8 mice per group). $^{*}P < 0.05$, (**E**) The quantitation of CD31-stained area in corneal flat mounts staining 6 dpi (n = 4 mice per group). $^{*}p < 0.05$. (**F**) Representative dot plots of the percentage of CD11b^{+} Ly6G^{+} cells in corneas. (**G**) Percentage of CD11b^{+} Ly6G^{+} cells in the cornea in WT mice or TRPM8$^{-/-}$ mice after topical treatment with menthol or control solution 2 dpi (n = 4 mice per group). $^{*}P < 0.05$.

downregulated in the corneas of TRPM8$^{-/-}$ mice after HSV-1 infection (Fig. 6B). The expressions of ISGs related to immune and inflammatory regulation were confirmed by qPCR verification, such as *Oas1a, Ccl5, Irf7, Mx1, H2-M3, Rsad2* were downregulated (Fig. 6C).

Therapeutic Effect of a TRPM8 Agonist Upon Corneal Inflammation After HSV-1 Infection

The subconjunctival injection of TRPM8 agonist menthol affects the symptoms of HSK in WT mice, but not in TRPM8$^{-/-}$ mice (Figs. 7A–C). Menthol diminished corneal pixel intensity on AS-OCT images (92.8 ± 5.434 in WT mice and 134.2 ± 4.897 in TRPM8$^{-/-}$ mice), compared with mice that treated with control solution in WT mice (109.7 ±3.972 in WT mice and 140.4 ± 3.832 in TRPM8$^{-/-}$ mice) (Fig. 7D). The subconjunctival injection of menthol also resulted in a significant reduction in angiogenesis 6 dpi (Fig. 7E and Supplementary Fig. S6) (26.59% ± 1.506% in the control group; 9.958% ± 1.2% in the menthol group in WT mice). In contrast, knockdown of TRPM8 abolished this effect (45.66% ± 7.144% in the control group; 40.86% ± 3.986% in menthol group in TRPM8$^{-/-}$ mice). Subconjunctival administration of menthol resulted in a decrease in the CD11b^{+} Ly6G^{+} cells ratio in the WT mice cornea (22.96% ± 1.271% in control group; 10.23% ± 1.554% menthol group) but not in TRPM8$^{-/-}$ mice (44.09% ± 3.353% in the control group; 42.77% ± 4.272% in menthol group) 2 dpi (Figs. 7F, 7G).

Discussion

In this study, we investigated the impact of TRPM8 dysfunction on HSK. The pathogenesis of HSK involves a complex interplay between the virus and the host immune response.[2,35] From the perspective of inflammation and pathogenicity, our findings indicate that the loss of TRPM8 promoted corneal inflammation and increased viral load on cornea. These changes might be closely associated with the accumulation of CD11b^{+} Ly6G^{+} cells and the downregulation of interferon signaling pathways, respectively.

TRPM8 exhibits both anti-inflammatory and proinflammatory properties.[36] Unlike its promotion of bronchiolitis[11] and liver fibrosis,[37] activation of TRPM8 exhibits a antinociceptive effect in mouse colitis models,[12–14] imiquimod-induced psoriasis-like inflammation,[10] Freund's complete adjuvant-induced inflammatory pain, and LPS-induced pulmonary inflammation.[20] In present study, we found that the loss of TRPM8 function led to increased corneal inflammation after infection, characterized by the accumulation of CD11b^{+} Ly6G^{+} cells along with elevated levels of chemokines and inflammatory cytokines. Neutrophils, as the "first responders" of white blood cells, are recruited to the infected area upon initial HSV-1 infection.[38,39] Research indicates that members of the TRP superfamily play a role in the migration and chemotaxis of neutropils.[40] Deletion of TRPC1 channels leads to impaired the impairment of neutrophil migration, transmigration, and chemotaxis.[41] Similarly, deficiency in TRPC6 hampers neutrophil recruitment,[42] as well as AKT and MAPK phosphorylation downstream of CXCR2 activation.[43] Furthermore, peripheral neurons expressing TRPV1 receptors suppressed the recruitment and surveillance of neutrophils via calcitonin gene-related peptide.[44,45] These findings suggest that the influence of TRPM8 on CD11b^{+} Ly6G^{+} cell recruitment may be specific to certain cell types, and dependent on the localization of expressing cells such as neurons, immune cells, or epithelial cells. Additionally, interplay between TRP channels may also play a crucial role in regulating neutrophil recruitment. Therefore further investigation is necessary for a comprehensive

Investigative Ophthalmology & Visual Science

understanding of the underlying mechanisms. In addition to the discussion of CD11b$^+$ Ly6G$^+$ cells, the Th1 and Th17 CD4$^+$ T cells also play a major role in HSK.[46–49] Studies have indicated that inhibiting TRPM8 during the T-cell activation may result in altered phenotype and reduced proliferation.[19] The roles of the Th1 and Th17 CD4$^+$ T cells in effect of TRPM8 functional loss on HSK remain to be explored.

Our study also found elevated corneal viral titers and decreased expression of ISG in TRPM8$^{-/-}$ mice after HSV-1 infection. Given that ISG products provide an antiviral state in cells,[35,50] these results indicated a potential impairment of the antiviral response in TRPM8$^{-/-}$ mice. In previous studies, we found that the corneas of TRPM8$^{-/-}$ mice with repetitive injuries showed squamous metaplasia, which may be related to the upregulation of interferon signals and the expression of ISG.[6] However, analyzing mice that had not undergone injury revealed that the expression of ISG in the corneas of TRPM8$^{-/-}$ mice was downregulated compared to WT mice (Supplementary Fig. S5), consistent with the findings presented in this study. This contradictory phenomenon represents a fascinating discovery, necessitating further investigations to elucidate the implications and underlying mechanisms of this finding. On the other hand, recent research has shown that the activation of TRPM8 stabilizes the level of mitochondrial antiviral signaling to promote resistance to Coxsackievirus B3 infection.[21] The increase in virus titers in TRPM8$^{-/-}$ mice may also be related to changes in other antiviral signals. In conclusion, this study highlights the importance of TRPM8 channels in the pathogenesis of HSK and suggests that TRPM8 agonists could be potential therapeutic agents for the management of HSK.

Acknowledgments

The authors thank Fangying Song, Qun Wang and Ya Li (Eye Institute of Shandong First Medical University) for participating in discussions surrounding this work.

Supported by the Natural Science Foundation of Shandong Province (ZR2020QH143, ZR2020QH142 and ZR2020QH144), the National Natural Science Foundation of China (82000851 and 82101094), Taishan Scholar Program (202211342), the Key Research and Development Program of Shandong Province (2021ZDSYS14) and Academic Promotion Program and Innovation Project of Shandong First Medical University (2019ZL001 and 2019RC008).

Disclosure: **J. Feng**, None; **L. Yang**, None; **L. Ran**, None; **X. Qi**, None; **X. Wang**, None; **Y. Zhang**, None; **Z. Zou**, None; **T. Liu**, None; **X. Wang**, None; **Y. Yu**, None; **X. Sun**, None; **Q. Zhou**, None

References

1. Lobo A, Agelidis A, DJTos Shukla. Pathogenesis of herpes simplex keratitis: the host cell response and ocular surface sequelae to infection and inflammation. *Ocul Surf*. 2019;17:40–49.
2. Rowe AM, St Leger AJ, Jeon S, et al. Herpes keratitis. *Progress in retinal and eye research*. 2013;32:88–101.
3. Quallo T, Vastani N, Horridge E, et al. TRPM8 is a neuronal osmosensor that regulates eye blinking in mice. *Nat Commun*. 2015;6:7150.
4. Parra A, Madrid R, Echevarria D, et al. Ocular surface wetness is regulated by TRPM8-dependent cold thermoreceptors of the cornea. *Nature Med*. 2010;16:1396–1399.
5. Yoon HJ, Kim J, Yang JM, et al. Topical TRPM8 agonist for relieving neuropathic ocular pain in patients with dry eye: a pilot study. *J Clin Med*. 2021;10.
6. Ran L, Feng J, Qi X, et al. Effect of TRPM8 functional loss on corneal epithelial wound healing in mice. *Invest Ophthalmol Vis Sci*. 2023;64:19.
7. Yang JM, Wei ET, Kim SJ, et al. TRPM8 channels and dry eye. *Pharmaceuticals (Basel, Switzerland)*. 2018;11.
8. Kaido M, Inoue S, Kawashima M, et al. Role of transient receptor potential melastatin 8 activity in menthol-induced cold sensitivity and its qualitative perception in dry eye. *Ocul Surf*. 2021;19:307–312.
9. Arcas JM, González A, Gers-Barlag K, et al. The immunosuppressant macrolide tacrolimus activates cold-sensing TRPM8 channels. *J Neurosci*. 2019;39:949–969.
10. Wang W, Wang H, Zhao Z, et al. Thymol activates TRPM8-mediated Ca(2+) influx for its antipruritic effects and alleviates inflammatory response in Imiquimod-induced mice. *Toxicol Appl Pharmacol*. 2020;407:115247.
11. Li M, Li Q, Yang G, et al. Cold temperature induces mucin hypersecretion from normal human bronchial epithelial cells in vitro through a transient receptor potential melastatin 8 (TRPM8)-mediated mechanism. *J Allergy Clin Immunol*. 2011;128:626–634.e621-625.
12. Ramachandran R, Hyun E, Zhao L, et al. TRPM8 activation attenuates inflammatory responses in mouse models of colitis. *Proc Natl Acad Sci USA*. 2013;110:7476–7481.
13. de Jong PR, Takahashi N, Peiris M, et al. TRPM8 on mucosal sensory nerves regulates colitogenic responses by innate immune cells via CGRP. *Mucosal Immunol*. 2015;8:491–504.
14. Khalil M, Babes A, Lakra R, et al. Transient receptor potential melastatin 8 ion channel in macrophages modulates colitis through a balance-shift in TNF-alpha and interleukin-10 production. *Mucosal Immunol*. 2016;9:1500–1513.
15. Taylor DJR, Hamid SM, Andres AM, et al. Antiviral effects of menthol on coxsackievirus B. *Viruses*. 2020;12.
16. Hornsby E, King HW, Peiris M, et al. The cation channel TRPM8 influences the differentiation and function of human monocytes. *J Leukocyte Biol*. 2022;112:365–381.
17. Khalil M, Babes A, Lakra R, et al. Transient receptor potential melastatin 8 ion channel in macrophages modulates colitis through a balance-shift in TNF-alpha and interleukin-10 production. *Mucosal Immunol*. 2016;9:1500–1513.
18. Kume H, Tsukimoto M. TRPM8 channel inhibitor AMTB suppresses murine T-cell activation induced by T-cell receptor stimulation, concanavalin A, or external antigen restimulation. *Biochem Biophys Res Commun*. 2019;509:918–924.
19. Acharya TK, Tiwari A, Majhi RK, et al. TRPM8 channel augments T-cell activation and proliferation. *Cell Biol Int*. 2021;45:198–210.
20. Caceres AI, Liu B, Jabba SV, et al. Transient receptor potential cation channel subfamily M member 8 channels mediate the anti-inflammatory effects of eucalyptol. *Br J Pharmacol*. 2017;174:867–879.
21. Alliger K, Khalil M, König B, et al. Menthacarin attenuates experimental colitis. *Phytomedicine*. 2020;77:153212.
22. Astani A, Reichling J, Schnitzler P. Comparative study on the antiviral activity of selected monoterpenes derived from essential oils. *Phytotherapy Res*. 2010;24:673–679.
23. Lai WL, Chuang HS, Lee MH, et al. Inhibition of herpes simplex virus type 1 by thymol-related monoterpenoids. *Planta Med*. 2012;78:1636–1638.
24. Müller J, Greiner JF, Zeuner M, et al. 1,8-Cineole potentiates IRF3-mediated antiviral response in human stem cells and in an ex vivo model of rhinosinusitis. *Clin Sci*. 2016;130:1339–1352.

25. Montgomery ML, Callegan MC, Fuller KK, et al. Ocular glands become infected secondarily to infectious keratitis and play a role in corneal resistance to infection. *J Virol*. 2019;93(16):e00314–e00319.
26. Morris J, Stuart PM, Rogge M, et al. Recurrent herpetic stromal keratitis in mice, a model for studying human HSK. *J Vis Exp*. 2012;(70):e4276.
27. Twardy BS, Channappanavar R, Suvas S. Substance P in the corneal stroma regulates the severity of herpetic stromal keratitis lesions. *Invest Ophthalmol Vis Sci*. 2011;52:8604–8613.
28. Tian X, Wang T, Zhang S, et al. PEDF reduces the severity of herpetic simplex keratitis in mice. *Invest Ophthalmol Vis Sci*. 2018;59:2923–2931.
29. Rose JS, Eldrina J, Joshua A, et al. Objective quantification of corneal haziness using anterior segment optical coherence tomography. *J Curr Ophthalmol*. 2018;30:54–57.
30. Dohlman TH, Yin J, Dana R. Methods for assessing corneal opacity. *Semin Ophthalmol*. 2019;34:205–210.
31. Piret J, Boivin G. Immunomodulatory strategies in herpes simplex virus encephalitis. *Clin Microbiol Rev*. 2020;33(2):e00105–e00119.
32. Wang L, Wang R, Xu C, et al. Pathogenesis of herpes stromal keratitis: immune inflammatory response mediated by inflammatory regulators. *Front Immunol*. 2020;11:766.
33. Azher TN, Yin XT, Stuart PM. Understanding the role of chemokines and cytokines in experimental models of herpes simplex keratitis. *J Immunol Res*. 2017;2017:7261980.
34. Liew PX, Kubes P. The neutrophil's role during health and disease. *Physiol Rev*. 2019;99:1223–1248.
35. Verzosa AL, McGeever LA, Bhark SJ, et al. Herpes simplex virus 1 infection of neuronal and non-neuronal cells elicits specific innate immune responses and immune evasion mechanisms. *Front Immunol*. 2021;12:644664.
36. Silverman HA, Chen A, Kravatz NL, et al. Involvement of neural transient receptor potential channels in peripheral inflammation. *Front Immunol*. 2020;11:590261.
37. Liu Q, Lei X, Cao Z, et al. TRPM8 deficiency attenuates liver fibrosis through S100A9-HNF4α signaling. *Cell Biosci*. 2022;12:58.
38. Sendra VG, Tau J, Zapata G, et al. Polluted air exposure compromises corneal immunity and exacerbates inflammation in acute herpes simplex keratitis. *Front Immunol*. 2021;12:618597.
39. Thomas J, Gangappa S, Kanangat S, et al. On the essential involvement of neutrophils in the immunopathologic disease: herpetic stromal keratitis. *J Immunol*. 1997;158:1383–1391.
40. Immler R, Simon SI, Sperandio M. Calcium signalling and related ion channels in neutrophil recruitment and function. *Eur J Clin Invest*. 2018;48(Suppl 2):e12964.
41. Lindemann O, Strodthoff C, Horstmann M, et al. TRPC1 regulates fMLP-stimulated migration and chemotaxis of neutrophil granulocytes. *Biochim Biophys Acta*. 2015;1853:2122–2130.
42. Damann N, Owsianik G, Li S, et al. The calcium-conducting ion channel transient receptor potential canonical 6 is involved in macrophage inflammatory protein-2-induced migration of mouse neutrophils. *Acta Physiol*. 2009;195:3–11.
43. Lindemann O, Umlauf D, Frank S, et al. TRPC6 regulates CXCR2-mediated chemotaxis of murine neutrophils. *J Immunol*. 2013;190:5496–5505.
44. Baral P, Umans BD, Li L, et al. Author correction: nociceptor sensory neurons suppress neutrophil and $\gamma\delta$ T cell responses in bacterial lung infections and lethal pneumonia. *Nat Med*. 2018;24:1625–1626.
45. Pinho-Ribeiro FA, Baddal B, Haarsma R, et al. Blocking neuronal signaling to immune cells treats streptococcal invasive infection. *Cell*. 2018;173:1083–1097.e1022.
46. Rajasagi NK, Rouse BT. The role of T cells in herpes stromal keratitis. *Front Immunol*. 2019;10:512.
47. Doymaz MZ, Rouse BT. Herpetic stromal keratitis: an immunopathologic disease mediated by CD4+ T lymphocytes. *Invest Ophthalmol Vis Sci*.. 1992;33:2165–2173.
48. Niemialtowski MG, Rouse BT. Predominance of Th1 cells in ocular tissues during herpetic stromal keratitis. *J Immunol*. 1992;149:3035–3039.
49. Lobo AM, Agelidis AM, Shukla D. Pathogenesis of herpes simplex keratitis: the host cell response and ocular surface sequelae to infection and inflammation. *Ocul Surf*. 2019;17:40–49.
50. Chew T, Taylor KE, Mossman KL. Innate and adaptive immune responses to herpes simplex virus. *Viruses*. 2009;1:979–1002.

Investigative Ophthalmology & Visual Science